MDPI

Assessing and Comparing Reference Evapotranspiration across Different Climatic Regions of China Using Reanalysis Products

Xingjiao Yu [1,2,†], Long Qian [1,2,†] , Wen'e Wang [1,2,*], Xuefei Huo [1,2], Xiaotao Hu [1,2] and Yafei Wang [1,2]

[1] Key Laboratory of Agricultural Soil and Water Engineering in Arid and Semiarid Areas,
Ministry of Education, Northwest A&F University, Yangling District, Xianyang 712100, China;
yxj0204@nwafu.edu.cn (X.Y.); qianlong9611@126.com (L.Q.); hxf@nwafu.edu.cn (X.H.);
huxiaotao11@nwsuaf.edu.cn (X.H.); wangyafei0222@163.com (Y.W.)

[2] College of Water Resources and Architectural Engineering, Northwest A&F University, Yangling District,
Xianyang 712100, China

[*] Correspondence: wangwene@nwsuaf.edu.cn

[†] These authors contributed equally to this work.

Abstract: This study aims to assess the accuracy of the reference evapotranspiration (ET_0) estimated by CLDAS, ERA5 reanalysis products, and the quality of reanalysis weather variables required to calculate PM-ET_0. For this purpose, the applicability of surface meteorological elements from the ERA5 reanalysis datasets provided by the European Centre for Medium-Range Weather Forecasts (ECMWF), and the second-generation China Meteorological Administration Land Data Assimilation System (CLDASV2.0) datasets are evaluated in China by comparison with local observations from 689 stations reported by the Chinese Meteorological Administration (CMA). Statistics including percent bias (PBias), coefficient of determination (R^2), root mean square error (RMSE) and mean absolute error (MAE) are used to check the accuracy. The results show the highest correlation between reanalysis temperature and observations, with a mean R^2 of 0.96, 0.90 for the CLDAS maximum and minimum air temperatures, and 0.87, 0.84 for ERA5. For the reanalysis of solar radiation (R_s) and relative humidity (RH), an overestimation trend is shown for R_s and an underestimation trend is shown for RH. For reanalysis of wind speed, a relatively low accuracy is shown. The accuracy of ET_0 estimated by the two reanalysis products is acceptable in China, but the spatial and temporal consistency between the CLDAS estimates and site observations is higher, with a mean RMSE R^2 of 0.91, 0.82 for CLDAS and 1.42, 0.70 for ERA5, respectively. Moreover, CLDAS reanalysis products are more effective in describing the boundary details of the study area.

Keywords: CLDAS reanalysis products; ERA5 reanalysis products; accuracy indicators; meteorological variables; reference evapotranspiration

1. Introduction

Evapotranspiration (ET) is an important meteorological element in the hydrological cycle, which is directly related to the energy and water balance of the Earth's surface, determining the formation and evolution of the geographical environment [1], and also an important basis and a key link in the evaluation of agricultural water use efficiency [2,3]. As the global competition for water resources intensifies and water resources become depleted, coping with water scarcity requires a more accurate knowledge of ET [4].

Irrigation management in agricultural practices requires the accurate estimation of crop water consumption, which in turn requires an accurate estimation of crop evapotranspiration (ET_c), and its forecasting is significant in developing crop irrigation systems and real-time irrigation scheduling [5,6]. A commonly used ET_c estimation method at the field scale consists of using the Kc-ET_0 approach, as proposed in FAO56 [7], where a crop coefficient (K_c) for the considered vegetation is multiplied by the crop reference

evapotranspiration (ET_0) to estimate the ET_c, although the calculation of K_c is based on experience, and applications worldwide are successful [8–10].

At present, ET_0 can also be estimated from pan evaporation, but such methods are expensive, technically complex, and not practical. Therefore, the Penman–Monteith model is usually used for the estimation ET_0 [11–14]. However, the model requires the input of several climate variables, including the maximum and minimum air temperature (T_{max} and T_{min}), relative humidity (RH), solar radiation (R_s), and wind speed at 2 m height (U_2). These variables are not observed, or the price of obtaining these meteorological data from the relevant meteorological services is prohibitive in many regions and locations in China. In addition, the common method of obtaining these meteorological data is station monitoring, which is time-consuming and makes it difficult to obtain long time series and high-quality meteorological variables.

Since the 1960s, the application of meteorological satellite data made up for the shortage of station observations, and the spatial and temporal continuity of meteorological data made great progress. After the 1990s, satellite data entered the data assimilation system, which further improved the accuracy of meteorological data [15,16]. Reanalysis information assimilates data obtained from remote sensing, ground-based observations and numerical simulations [17,18], which has the characteristics of high spatial and temporal resolutions and is an ideal driving data source for distributed models. The main advantage of reanalysis products is the free access to continuous meteorological data and its great advantage and potential to become an alternative to observed data.

Several global reanalysis datasets are available for ET_0 estimation, such as WorldClim, which provides the global historical and future climate data and elevation data [19]; The World Meteorological Organization's Climate Explorer weather data retrieval platform, with a wealth of global or regional climate data [20]; the European Centre for Medium-range Weather Forecasts (ECMWF), which provides ERA5 reanalysis products [21]; the National Centers for Environmental Prediction/National Center for Atmospheric Research (NCEP/NCAR), known as NCEP/NCAR Reanalysis I [22]; the National Aeronautics and Space Administration (NASA) Global Simulation; and the Assimilation Office for a Second Review of Modern Research and Applications (MERRA-2) [23,24], etc.

The main advantages of the reanalysis product are the high spatial and temporal resolutions, the ability to scale the product appropriately, and the stable improved model resolution and bias [25]. Currently, many authors have used reanalysis products to represent the spatiotemporal variability of surface climate variables. ERA5_land reanalysis data were applied to the observations of Peruvian glaciers verified by Martin et al., and were found to be appropriate for characterizing 2 m air temperature and relative humidity, particularly in the wet outer tropics [26]. Song et al. (2020) [27] compared the applicability of various soil moisture data in Inner Mongolia, and found that the ERA5 simulation capability is optimal. Srivastava et al. (2016) [28] compared the ET_0 estimation from ERA-interim and NCEP for all the seasons, and revealed a similar performance to the seasonal assessment, with a higher agreement for the ERA-interim. The only drawback of using a downscaling ERA-interim reanalysis dataset with the WRF is that it is time-consuming. Martins et al. (2016) [29] used the ERA-interim and NOAA NCEP reanalysis datasets for the calculation of PM-ET_0 in the Iberian Peninsula and compared it with the ET_0 Observed at 130 meteorological stations in the Iberian Peninsula. The results supported the quality of the ERA-interim reanalysis data to calculate the ET_0 computations. The ECMWF ERA5 reanalysis products were selected for this study because they had previously performed well and showed great a potential for estimating ET_0. However, due to the bias reported for ERA products, the use of these data requires assessing the impact of bias on the performance of the estimations of reanalysis-based ET_0 when compared with ET_0 computed with observational data [30,31].

CLDAS-V2.0 is the latest version of the land surface assimilation system developed by the China National Meteorological Information Center, providing a variety of atmospheric driving field products (URL: https://data.cma.cn/, accessed on 1 May 2021). At the same

time, some scholars have evaluated the applicability of different land surface model data. Liu et al. (2021) [32] compared CLDAS air temperature data with hourly air temperature data from 48,708 ground automatic meteorological stations in China for 2017–2018, and found that CLDAS air temperature data better reflects the interannual variability of air temperature in Chinese regions, with an average correlation coefficient of more than 0.991. Shi et al. (2018) [33] analyzed the temporal variation characteristics of average soil moisture in China by comparing CLDAS soil moisture with hourly observations of automatic soil moisture observation stations, concluding that the simulated values were very close to the observed values, and the time-series variation of soil moisture was captured in each study area. Using GLDAS and CLDAS forcing data, Yang et al. (2017) [34] evaluated precipitation and shortwave radiation from the ITPCAS, GLDAS, CLDAS and the gridded analysis based on CMA gauge observations (CN05.1) over mainland China during 2008–2014, and showed that CLDAS provides more realistic precipitation and radiation approximations than the other datasets. The CLDAS forcing dataset contains more in situ and remote sensing observations of China, so it is more accurate over mainland China. Liu et al. (2019) [35] compared and evaluated the simulation results of monthly soil moisture and monthly evapotranspiration, and reported that CLDAS_Noah-MP significantly improved the simulation results for mainland China and eight river basins; the R-value increased from 0.451 to 0.534 and the RMSE reduced from 0.078 to 0.068, which confirmed the superiority of CLDAS, as previously reported by Cui et al. (2018) [36] and Shi et al. (2018) [37].

The most recent studies have focused on assessing one or several meteorological variables for the reanalysis of atmospheric field-driven products, but relatively few have conducted comprehensive assessments of the meteorological variables required to calculate ET_0 and reanalysis for ET_0 estimation, especially for small temporal scales. In addition, the numerical–physical approach, horizontal and vertical resolution, and temporal variability of the reanalysis model will bring uncertainties in the reanalysis simulation process [38,39]. The resolution and accuracy of these reanalysis products appear to vary with the location and timescale of the study [40]. Although research indicates that the spatial resolution and reliability of the new generation of reanalysis data products have improved, there is still a need to evaluate the region-specific applicability of CLDASV2.0, ERA5 reanalysis weather variables and the estimation of ET_0 in different climate zones of China, and find the best method for researchers and users to carry out irrigation practices.

The main objective of this research is to apply the ET_0 calculated from reanalysis data to irrigation scheduling and management, for which it can be used in those places where the weather data quality is low or (and) weather variables are missing [41,42]. The correlations and bias of the five reanalyzed meteorological variables from CLDASV2.0 and ERA5 are compared based on the daily weather variable data obtained from 689 ground automatic meteorological stations in China from 2017–2019. Any biases in these products can be identified by comparison so that the bias correction method can be easily applied. Moreover, a comprehensive set of the statistical indicators is used to assess how calculated reanalysis PM-ET_0 compared with the corresponding station observations, which also offers a reference for the selection and application of CLDASV2.0 and ERA5 reanalysis meteorological data across different climatic regions of China.

2. Materials and Methods

2.1. Meteorological Data

CLDAS uses fusion and assimilation technology to fuse data from various sources, such as ground observation, satellite observation, numerical model products and numerical model products, then output the land surface-driven products with high spatial and temporal resolution, including the maximum and minimum air temperatures, 2 m specific humidity, 10 m wind speed, etc. It covers the Asian region (60°–160° E, 0°–65° N), with a spatial resolution of 0.0625° × 0.0625° and a temporal resolution of 1 h. The dataset is formed by using the ECMWF numerical analysis/forecasting product as the background field and the topographic adjustment, multigrid variational assimilation, optimal interpola-

tion and other techniques in the Chinese region, to fuse the ground-based automatic station observations and interpolate them to the reanalysis grid points [33,43].

ERA5 is the fifth generation of ECMWF atmospheric reanalysis of the global climate, created by the EU-funded Copernicus Climate Change Service (C3S). It assimilates remote sensing information, upper atmosphere, and near-surface conventional observation data, including different regions and sources, on a global scale, spanning from 1979 to the present, achieving real-time updates with a spatial resolution of $0.25° \times 0.25°$ latitude-longitude [44]. ERA5 reanalysis data provide many kinds of meteorological elements, including 2 m air temperature, 2 m dew point temperature, and 10 m wind speed, etc. The data sources can be found at http://cdds.climate.copernicus.eu/.

2.2. FAO-56 Penman–Monteith Equation

The reference crop evapotranspiration was calculated using the FAO-56 Penman–Monteith equation recommended by the Food and Agriculture Organization of the United Nations (FAO) in 1998 and the PM-ET_0 Equation (1). It is not an empirical equation, but a mechanistic combination equation derived from the definition of the Penman–Monteith equation, parameterized for the reference crops [45]. ET_0 (mm day^{-1}) is described as follows.

$$ET_0 = \frac{0.408\Delta(R_n - G) + \gamma\frac{900}{T_a+273}u_2(e_s - e_a)}{\Delta + \gamma(1 + 0.34u_2)} \tag{1}$$

where ET_0 is the reference crop evapotranspiration (mm d^{-1}), R_n is the net radiation at the crop surface (MJ m^{-2} day^{-1}) and G is the soil heat flux density (MJ m^{-2} day^{-1}). T_a is the mean daily air temperature at 2 m height (°C) calculated from the maximum and minimum air temperature (T_{max} and T_{min}, °C), u_2 is the wind speed at 2 m height (m s^{-1}), e_s is the saturated vapor pressure (kPa), e_a is actual water vapor pressure (kPa), $e_s - e_a$ is the vapor pressure deficit (kPa) calculated from the saturation vapor pressure and actual vapor pressure, Δ is the slope of the vapor pressure curve (kPa °C^{-1}) and γ is the psychrometric constant (kPa °C^{-1}). In the daily calculation scale, G is small relative to R_n, and is therefore neglected [46,47].

2.3. Data Sources

Station observation data were collected from 689 meteorological stations of the China Meteorological Administration (https://data.cma.cn/). The list of variables retrieved is defined by the Penman–Monteith model FAO56 framework, including the maximum and minimum air temperatures at 2 m, surface radiation, sunshine duration, relative humidity at 2 m and wind speed at 10 m. The data are subjected to quality control such as climate threshold value check, temporal consistency, and spatial consistency check.

ET_0 is significantly affected by seasonal variation and regional differences. The two types of data from the different time series and different study regions are compared in the study, and the detailed analysis and comparison are presented in Section 3. T_{max} and T_{min}, RH, R_s, U_2 and the estimated PM-ET_0 from CLDAS2.0, ERA5, and station observations in 2017–2019 in the Chinese region are selected as the research objects. China was divided into 7 climatic zones according to climatic characteristics and heat indexes [48,49]. Regions 1–7 are the Northwest desert zone, Inner Mongolia grassland zone, Northeast humid and semi-temperate zone, humid and semi-humid warm temperate zone, humid subtropical zone, humid tropical zone and the Qinghai Tibet Plateau zone (Figure 1). Bias, correlation, and error of the estimated PM-ET_0 across different climate zones and the CLDAS and ERA5 reanalysis weather variables used to estimate ET_0 are analyzed.

2.4. Spatial Interpolation Method

The meteorological variables related to the calculation of PM-ET_0 have been extracted from the CLDAS2.0, ERA5 reanalysis grid points, and then these grid point meteorological data were interpolated to the same latitude and longitude positions as the 689 ground observation sites, and the meteorological data obtained from the interpolation are evaluated

as true values for the test. Grid data from four grid points around it were selected and interpolated to the station by the inverse distance weight (IDW) method. The formula is as follows:

$$Z = \frac{\sum\limits_{i=1}^{n} \frac{Z_i}{D_i}}{\sum\limits_{i=1}^{n} \frac{1}{D_i}}$$

(2)

where Z is the true value, Z_i is the value of the control point, and D_i is the weight coefficient.
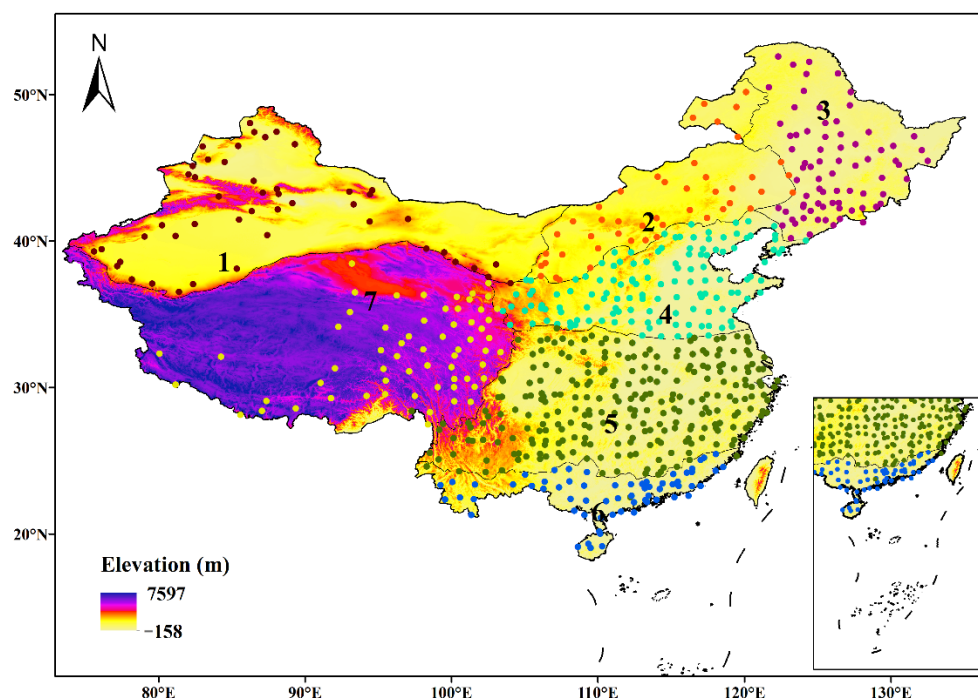
Figure 1. Spatial distribution of seven climatic zones in China and 689 utilized meteorological stations (The dots with different colors in the figure represent meteorological stations located in different climatic regions).

2.5. Accurate Statistical Indicators

The assessment focused on the pairwise comparison between the weather stations' observed values (Q_i) and the corresponding values (P_i) for the two reanalysis datasets for each meteorological variable used in ET_0 computations and for the ET_0 values [50]. The following several statistical indicators were used to assess the performance of the reanalysis datasets in representing the spatial and temporal variation of the meteorological variables.

The percent bias (PBias) measures the degree of deviation between the reanalysis estimated data and the corresponding site observations [51]. It is simply a normalized difference between the means of both sets of values: positive values indicate overestimation, and negative values indicate underestimation.

$$PBias = \frac{\sum\limits_{i=1}^{n} (P_i - Q_i)}{\sum\limits_{i=1}^{n} Q_i}$$

(3)

The coefficient of determination (R^2) is used to assess the degree of dispersion between the reanalysis estimated value and the site observations. The closer the R^2 is to 1, the

closer the actual site measurements are to the estimated and the higher the correlation, calculated as:

$$R^2 = \frac{\left[\sum\limits_{i=1}^{n} (Q_i - \overline{Q_i})(P_i - \overline{P_i})\right]^2}{\sum\limits_{i=1}^{n} (Q_i - \overline{Q_i})^2 \sum\limits_{i=1}^{n} (P_i - \overline{P_i})^2} \tag{4}$$

The root means square error (RMSE) measures the overall difference between the reanalysis estimated values and the site observations. Because of its high sensitivity to outliers, RMSE can better reflect the accuracy of the data.

$$RMSE = \sqrt{\frac{1}{n}\sum\limits_{i=1}^{n}(Q_i - P_i)^2} \tag{5}$$

The mean absolute error (MAE) is a measure of the error between the paired reanalysis estimated values and site observations, computed as:

$$MAE = \frac{1}{n}\sum\limits_{i=1}^{n}(Q_i - P_i)^2 \tag{6}$$

3. Results

3.1. Assessing the Accuracy of the Reanalysis Weather Variables

The assessment indicators PBias, RMSE, MAE and R^2 for the reanalysis estimated air temperatures ($T_{min\ CLDAS}$, $T_{max\ CLDAS}$, $T_{min\ ERA5}$, and $T_{max\ ERA5}$) and the corresponding observed values are summarized in Tables 1 and 2. Reanalysis T_{min} shows a trend of overestimation, with the average PBias of $T_{min\ CLDAS}$ and $T_{min\ ERA5}$ being 0.07 and 0.06, respectively. On the contrary, T_{max} reveals a trend of underestimation, and the mean PBias of $T_{max\ CLDAS}$ and $T_{max\ ERA5}$ are -0.06 and -0.34, respectively. When comparing the reanalysis T_{max}, the correlation between reanalysis T_{min} and site observations is higher, the average R^2 of the two reanalysis Tmin being 0.96, 0.87 and the corresponding R^2 values for reanalysis T_{max} 0.90, 0.84, but with a larger PBias in the case of T_{min}.

Table 1. Statistical indicators for the minimum air temperature when comparing CLDAS and ERA5 reanalysis products with the observed values across seven climatic zones and mainland China.

Climate Zones	$T_{min\ CLDAS}$				$T_{min\ ERA5}$			
	PBias	RMSE	MAE	R^2	PBias	RMSE	MAE	R^2
		(°C)				(°C)		
1	0.24	3.22	2.76	0.96	0.36	7.29	6.34	0.90
2	0.31	2.00	1.48	0.98	0.42	5.91	5.05	0.92
3	0.10	2.42	1.83	0.97	1.38	5.17	4.36	0.91
4	0.04	2.12	1.68	0.97	−0.65	9.47	8.51	0.88
5	−0.02	1.79	1.43	0.96	−0.57	13.54	12.33	0.86
6	−0.01	1.51	1.20	0.94	−0.53	16.85	15.40	0.80
7	−0.16	4.08	3.62	0.93	0.04	6.98	5.66	0.83
Average	0.07	2.45	2.00	0.96	0.06	9.32	8.24	0.87

T_{max} and T_{min} are the key meteorological factors to calculate ET_0. Therefore, RMSE, MAE and R^2 are further used to assess the error and correlation of the reanalysis air temperature. It can be seen from Tables 1 and 2 that the air temperature estimates of CLDAS and ERA5 products are consistent with the site observations, and the correlation values are between 0.76 and 0.98. Among the two products, CLDAS estimations are much closer to the observed values, with lower root means square error values (average range from 2.45 to 3.52) and higher correlation values (average range from 0.96 and 0.90) in most

climate zones compared to those obtained from ERA5 (average range from 9.32 to 9.66 and 0.87 to 0.84, respectively).

Table 2. Statistical indicators for the maximum air temperature when comparing CLDAS and ERA5 reanalysis products with the observed values across seven climatic zones and mainland China.

| Climate Zones	$T_{max\ CLDAS}$				$T_{max\ ERA5}$			
	PBias	RMSE	MAE	R^2	PBias	RMSE	MAE	R^2
		(°C)				(°C)		
1	−0.14	4.24	3.67	0.95	−0.32	8.40	7.35	0.87
2	−0.03	3.25	2.50	0.93	−0.29	6.31	5.41	0.90
3	−0.01	3.19	2.45	0.94	−0.28	5.56	4.64	0.89
4	−0.03	3.26	2.59	0.92	−0.37	10.14	8.86	0.83
5	−0.02	2.89	2.23	0.88	−0.41	12.75	11.01	0.79
6	−0.02	2.30	1.79	0.85	−0.43	15.09	13.07	0.76
7	−0.18	5.48	4.89	0.83	−0.28	9.38	7.88	0.82
Average	−0.06	3.52	2.87	0.90	−0.34	9.66	8.32	0.84

Four indicators of statistical accuracy of reanalysis solar radiation (R_s) across seven different climate zones and mainland China are shown in Table 3. The overall trends of the PBias, RMSE, MAE and R^2 for reanalysis $R_{s\ CLDAS}$ and $R_{s\ ERA5}$ are consistent, with differences in the numerical values. The mean R^2 of $R_{s\ CLDAS}$ is between 0.50 and 0.65, and the mean R^2 of $R_{s\ ERA5}$ is between 0.40 and 0.55, indicating that the reanalysis R_s agrees well with $R_{s\ Obs}$. However, reanalysis $R_{s\ CLDAS}$ better reflects the variability of the site-observed R_s in the overwhelming of locations compared to $R_{s\ ERA5}$. The bias of $R_{s\ CLDAS}$ and $R_{s\ ERA5}$ ranges from 0.02 to 0.17 and 0.06 to 0.24, demonstrating that both the reanalysis products slightly overestimate the observed R_s.

Table 3. Statistical indicators of solar radiation originated from CLDAS and ERA5 reanalysis products in different climate zones and mainland China.

Climate Zones	$R_{s\ CLDAS}$				$R_{s\ ERA5}$			
	PBias	RMSE	MAE	R^2	PBias	RMSE	MAE	R^2
		(MJ m^2 d^{-1})				(MJ m^2 d^{-1})		
1	0.02	4.04	2.87	0.65	0.06	4.31	3.47	0.53
2	0.06	4.21	2.95	0.60	0.11	4.43	3.50	0.51
3	0.04	4.16	2.91	0.58	0.13	4.22	3.31	0.55
4	0.14	4.84	3.38	0.53	0.15	5.23	3.92	0.46
5	0.10	4.78	3.40	0.54	0.24	5.08	4.01	0.41
6	0.17	4.33	3.16	0.51	0.18	4.63	3.58	0.38
7	0.02	4.46	3.25	0.50	0.09	4.54	3.47	0.40
Average	0.08	4.40	3.14	0.56	0.14	4.63	3.61	0.45

The spatial distribution of PBias, RMSE, MAE and R^2 of R_s across the different climatic regions of China are presented in Figure 2. The regional distribution of the statistical indicators of R_s is characterized clearly. The estimation bias and error are generally lower in the northwest and northeast regions than in the southeast; in other words, the mean PBias, RMSE and MAE are small in arid and semi-arid regions (climate zones 1, 2) and cold regions (climate zone 3), with distributions ranging from 0.02 to 0.13, 4.04 to 4.43 and 2.87 to 3.51, respectively. The average biases and estimation errors are large for humid and semi-humid areas (climate zones 4,5 and climate zone 6), with distributions of the PBias, RMSE and MAE ranging from 0.10 to 0.24, 4.33 to 5.23 and 3.16 to 4.01, respectively. The R^2 of R_s is the opposite of the previous three indicators. The R^2 of $R_{s\ CLDAS}$ and $R_{s\ ERA5}$ is between 0.65 and 0.58, and 0.55 and 0.50 in climatic zones 1, 2 and 3, while the R^2 is between 0.51 and

0.54 and 0.38 and 0.46 in climatic zones 4, 5 and 6. As a whole, the reanalysis of $R_{s \, CLDAS}$ and $R_{s \, ERA5}$ reflected the temporal and spatial variation characteristics of $R_{s \, Observed}$ well at most stations.
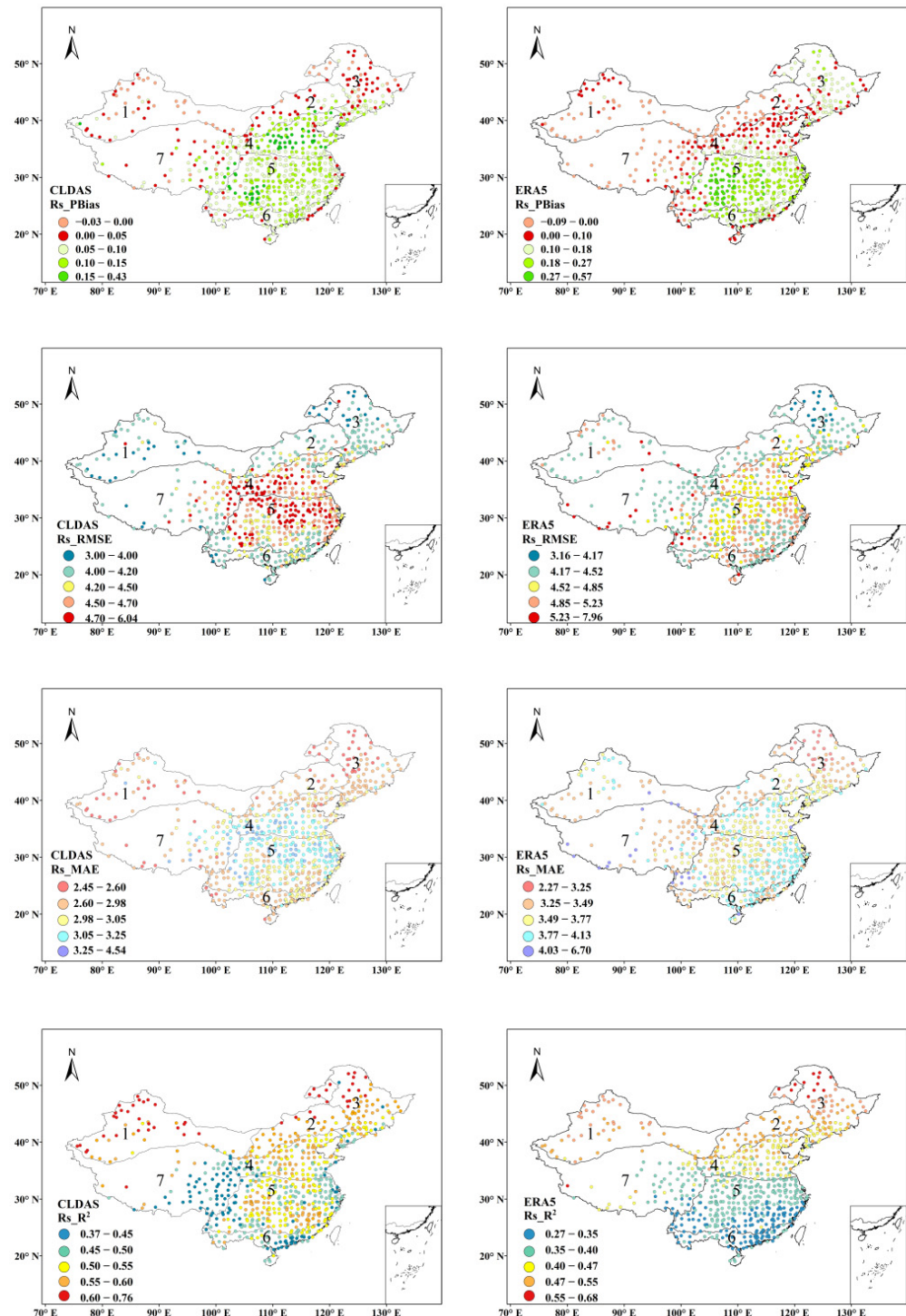
Figure 2. Spatial distribution of solar radiation percent bias (PBias), root mean square error (RMSE), mean absolute error (MAE) and the correlation coefficient (R^2) estimation with adopting CLDAS, ERA5, and station observation statistics.

The statistical indicators of reanalysis relative humidity are shown in Table 4. The PBias of RH_{CLDAS} is negative (ranging from −0.07 to −0.30) across the 1–6 climate zones. The results indicate a slight underestimation, with the PBias of climate zone 7 being positive,

with a value of 0.35. The PBias of RH_{ERA5} are 0.04 and 0.20 in climate zones 4 and 7, respectively, indicating a slight overestimation trend, and the remaining climate zones have a negative PBias, with values from −0.17 to −0.34. As for the error, compared with other climate zones, the estimation errors for climate zone 7 are larger, the RMSE and MAE for RH_{CLDAS} are 25.94% and 22.51%, respectively, and those of ERA5 are 22.70% and 18.84%. Reanalysis RH and the observed RH_{Obs} are in better agreement in climate zone 2, and the correlation values are 0.68 and 0.53 for RH_{CLDAS} and RH_{ERA5}, but the estimation error is relatively high, with the corresponding RMSE values of 11.63% and 18.51%. Furthermore, the estimation errors for climate zones 1–3 (RMSE between 10.82 and 21.75%) are generally larger than those for climate zones 4–6 (RMSE between 7.91 and 17.47%), partly because the latter are located in the humid zones with little variation in daily relative humidity, while the former are in the arid desert and grassland zones with a low vegetation cover and more frequent changes in daily relative humidity.

Table 4. Statistical indicators of relative humidity originated from CLDAS and ERA5 reanalysis products across different climate zones and mainland China.

| Climate Zones | RH_{CLDAS} | | | | RH_{ERA5} | | | |
| | PBias | RMSE | MAE | R^2 | PBias | RMSE | MAE | R^2 |
		(%)				(%)		
1	−0.30	12.84	10.29	0.58	−0.34	21.75	18.80	0.45
2	−0.29	11.63	9.79	0.68	−0.26	18.51	13.99	0.53
3	−0.20	10.82	8.23	0.59	−0.27	11.09	9.47	0.48
4	−0.14	8.71	7.13	0.63	0.04	15.46	11.60	0.46
5	−0.14	10.24	8.27	0.51	−0.17	17.47	13.08	0.41
6	−0.07	7.91	6.32	0.62	−0.21	14.83	10.17	0.48
7	0.35	25.94	22.51	0.37	0.20	22.70	18.84	0.32
Average	−0.12	12.58	10.36	0.57	−0.14	17.40	13.71	0.45

In contrast to the performance of the previous weather variables, both $U_{2\,CLDAS}$ and $U_{2\,ERA5}$ show a relatively low accuracy, with a high dispersion of pairs of 2 m wind speed derived from the reanalysis datasets and the station observations along the regression line, with R^2 averages of 0.25 for $U_{2\,CLDAS}$ and 0.18 for $U_{2\,ERA5}$. For PBias, $U_{2\,CLDAS}$ is underestimated relative to RH_{Obs}., and PBias ranged from −0.31 to −0.63 in seven different climatic regions. $U_{2\,ERA5}$ is underestimated in climate zones 1–3, with PBias ranging from −0.33 to −0.78, and overestimated in the rest of the climate zones with PBias ranging from 0.21 to 0.41. In terms of RMSE and MAE, the mean values of the RMSE and MAE are 1.09, 0.84 for $U_{2\,CLDAS}$ and 1.23, 0.99 for $U_{2\,ERA5}$ at the national scale, respectively, the details can be found in Table 5.

Table 5. Statistical indicators of wind speed originated from CLDAS and ERA5 reanalysis products across different climate zones of China.

| Climate Zones | $U_{2\,CLDAS}$ | | | | $U_{2\,ERA5}$ | | | |
| | PBias | RMSE | MAE | R^2 | PBias | RMSE | MAE | R^2 |
		(%)				(%)		
1	−0.50	1.31	0.98	0.26	−0.78	1.63	1.45	0.22
2	−0.47	1.52	1.08	0.30	−0.33	1.21	0.94	0.23
3	−0.63	0.90	0.68	0.31	−0.46	1.08	0.84	0.18
4	−0.31	0.90	0.66	0.23	0.41	1.15	0.90	0.15
5	−0.46	1.20	1.05	0.25	0.33	1.11	0.87	0.16
6	−0.42	1.13	0.94	0.21	0.21	1.39	1.10	0.18
7	−0.58	0.68	0.52	0.19	0.23	1.04	0.81	0.14
Average	−0.48	1.09	0.84	0.25	−0.06	1.23	0.99	0.18

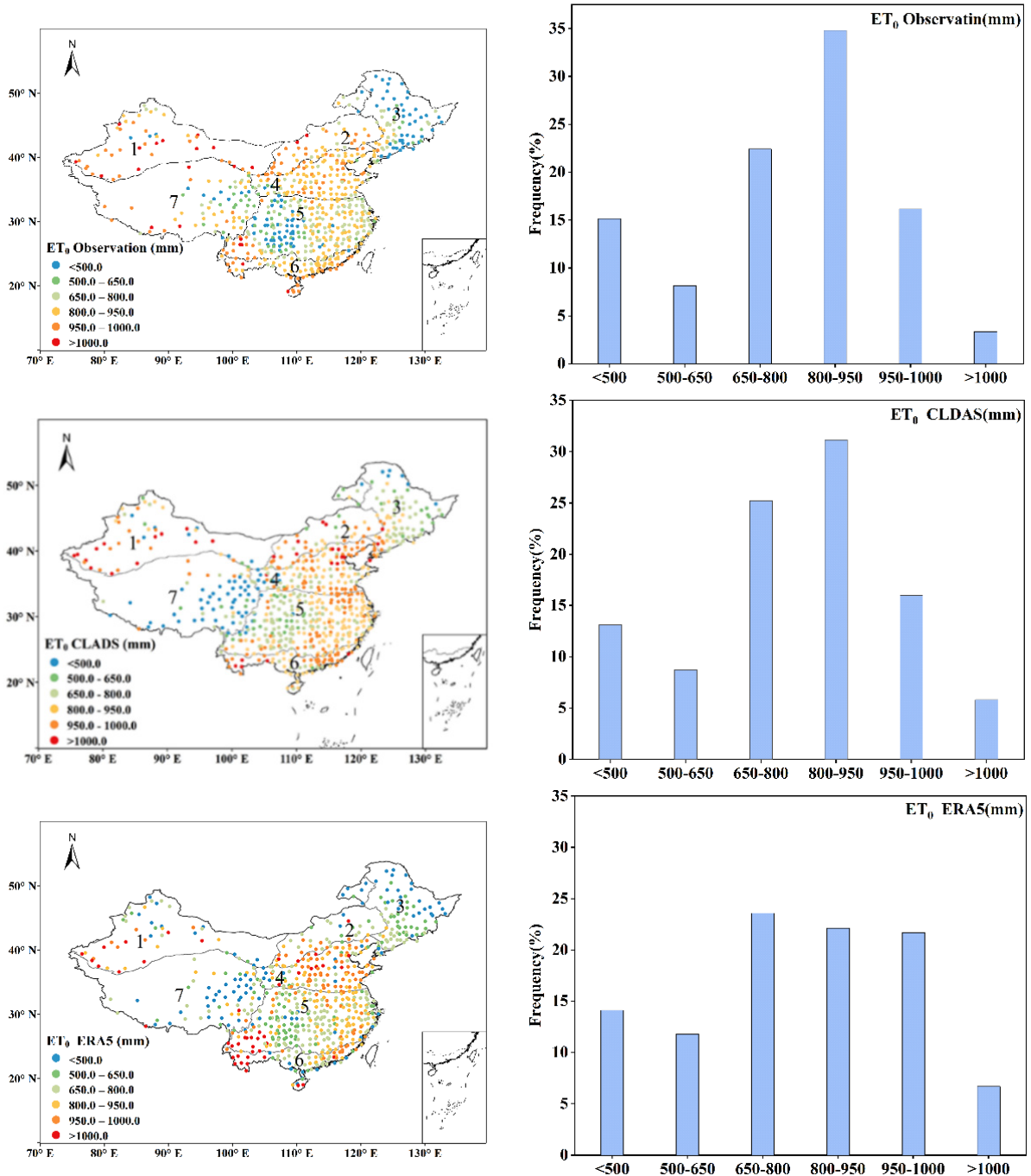*3.2. Comparison of the Annual Mean of the Observation-Calculated ET_0 and Reanalysis-Estimated ET_0*

A spatial distribution of the annual mean values of ET_0 calculated from the stations observations ($ET_{0\ Obs}$), ET_0 estimated by CLDAS ($ET_{0\ CLDAS}$), and ET_0 estimated by ERA5($ET_{0\ ERA5}$) in China, is shown in Figure 3. The frequency distribution of the average annual evapotranspiration between different value ranges is shown in the histogram of Figure 3. The spatial distribution of the annual mean values of ET_0 estimated from the two reanalysis datasets are approximately the same; however, from the perspective of frequency distribution, $ET_{0\ CLDAS}$ is more consistent with $ET_{0\ Obs}$. For the observed calculated ET_0, only 15.14% of stations have an $ET_{0\ Obs}$ < 500 mm, 23.41% of stations an $ET_{0\ Obs}$ between 650 and 800 mm, 16.15% of stations an $ET_{0\ Obs}$ between 950 and 1000 mm, and 3.34% of stations an $ET_{0\ Obs}$ > 1000 mm. For the CLDAS estimated ET_0, 13.10% of the stations showed $ET_{0\ CLDAS}$ <500 mm, $ET_{0\ CLDAS}$ ranged from 650 mm to 800 mm for 25.21% of the stations, from 800 mm to 900 mm for 15.97% of stations, and 5.82% of stations exhibited an $ET_{0\ CLDAS}$ >1000 mm. The frequency distribution of different intervals of the annual mean evapotranspiration estimated by CLDAS is similar to that of the site-observed ET_0, but in most cases, $ET_{0\ CLDAS}$ is slightly overestimated.

For ERA5 estimated ET_0, 11.79% of stations have an $ET_{0\ ERA5}$ between 500 and 650 mm, which is 3.64% higher than the frequency of $ET_{0\ Obs}$ observations in this range. Of the stations, 21.69% have $ET_{0\ ERA5}$ between 950 and 1000 mm, an increase of 5.53% over the percentage of $ET_{0\ Obs}$ in this interval, while the proportion of $ET_{0\ ERA5}$ with an annual average evapotranspiration interval in the range of 800–950 mm is lower than that of $ET_{0\ Obs}$. The frequency distribution of $ET_{0\ ERA5}$ in different evapotranspiration intervals differs from that of $ET_{0\ Obs}$ observations, and $ET_{0\ ERA5}$ is overall overestimated relative to the $ET_{0\ Obs}$ site-observed values.

The statistical indicators of ET_0 from station observations and two reanalysis estimates show significant regional variations in different climatic regions of China (Figure 4). The annual mean ET_0 in climate zones 1 and 2 is mainly concentrated between 800 and 950 mm, with a higher ET_0 in Xinjiang; for example, ET_0 is greater than 1000 mm in Urumqi and other stations. The annual mean ET_0 in climate zone 3 is low, with the lower values appearing in the eastern and northern parts of climate zone 3, and the lowest values of ET_0 in the whole of China also occur in this region, which may be caused by the lower average temperature. The majority of the stations in climate zone 4 have a small trend of annual mean ET_0 fluctuations and are concentrated in the range of 800–950 mm; however, ET_0 changes in the west of climate zone 4 and the southwest of climate zone 5, and its accuracy statistical indicators also change abruptly at this boundary location, and the change in $ET_{0\ CLDAS}$ is more significant, mainly because these two locations are susceptible to topography. The high fluctuation of ET_0 in climatic zones 6 and 7, where the higher PBias and RMSE values also occur (Figure 4), is due to the influence of the topography of the Tibetan Plateau region. In addition, the short sunshine time and high relative humidity cause a lower ET_0 in the southwestern part of climate zone 6 and the eastern part of climate zone 7. Compared with the ERA5 reanalysis data, CLDAS can better simulate the detailed characteristics of ET_0 in different climate zones.

To explore the accuracy of estimating the daily ET_0 from CLDAS, ERA5 reanalysis data for different climatic zones is shown. The paired comparisons between $ET_{0\ Obs}$ and $ET_{0\ CLDAS}$ (1st line, 3rd line), and $ET_{0\ Obs}$ and $ET_{0\ ERA5}$ are shown in scatter plots in Figure 5, in which all stations are from seven different climate zones. The analysis in Figure 5 complements the one in Figure 4 in detail. The results show that except for climate zone 7, the simulated ET_0 of the reanalysis datasets is closer to the $ET_{0\ Obs}$ of the stations in the arid and semi-arid areas; that is, the scatter points are concentrated on the y = x line, and the lowest value of the $ET_{0\ CLDAS}$ correlation value is 0.91, and the lowest value of the $ET_{0\ ERA5}$ correlation value is 0.85. The R^2 values of the two reanalysis products are smaller in humid, and sub-humid areas, ranging from 0.71 to 0.86, and 0.63 to 0.72 for $ET_{0\ CLDAS}$ and $ET_{0\ ERA5}$. The results indicate that the variability of meteorological variables is higher in humid and semi-humid areas than in arid and semi-arid areas. Moreover, the accuracy

of the reanalysis products for extreme weather estimation is low, and the extreme values of $ET_{0\,Obs}$ tend to be reconciled by the reanalysis datasets. For example, when the $ET_{0\,Obs}$ value at site 50,557 is greater than 6 mm d^{-1}, the reanalysis estimates ET_0 to be less than the corresponding site-observed ET_0 value. When the $ET_{0\,Obs}$ value at the sites is 59, 133 is less than 2 mm d^{-1}, and the ET_0 simulated by ERA5 is greater than the $ET_{0\,Obs}$erved at the corresponding site. These phenomena can be explained in the reanalysis temperature variables in Section 2.2.
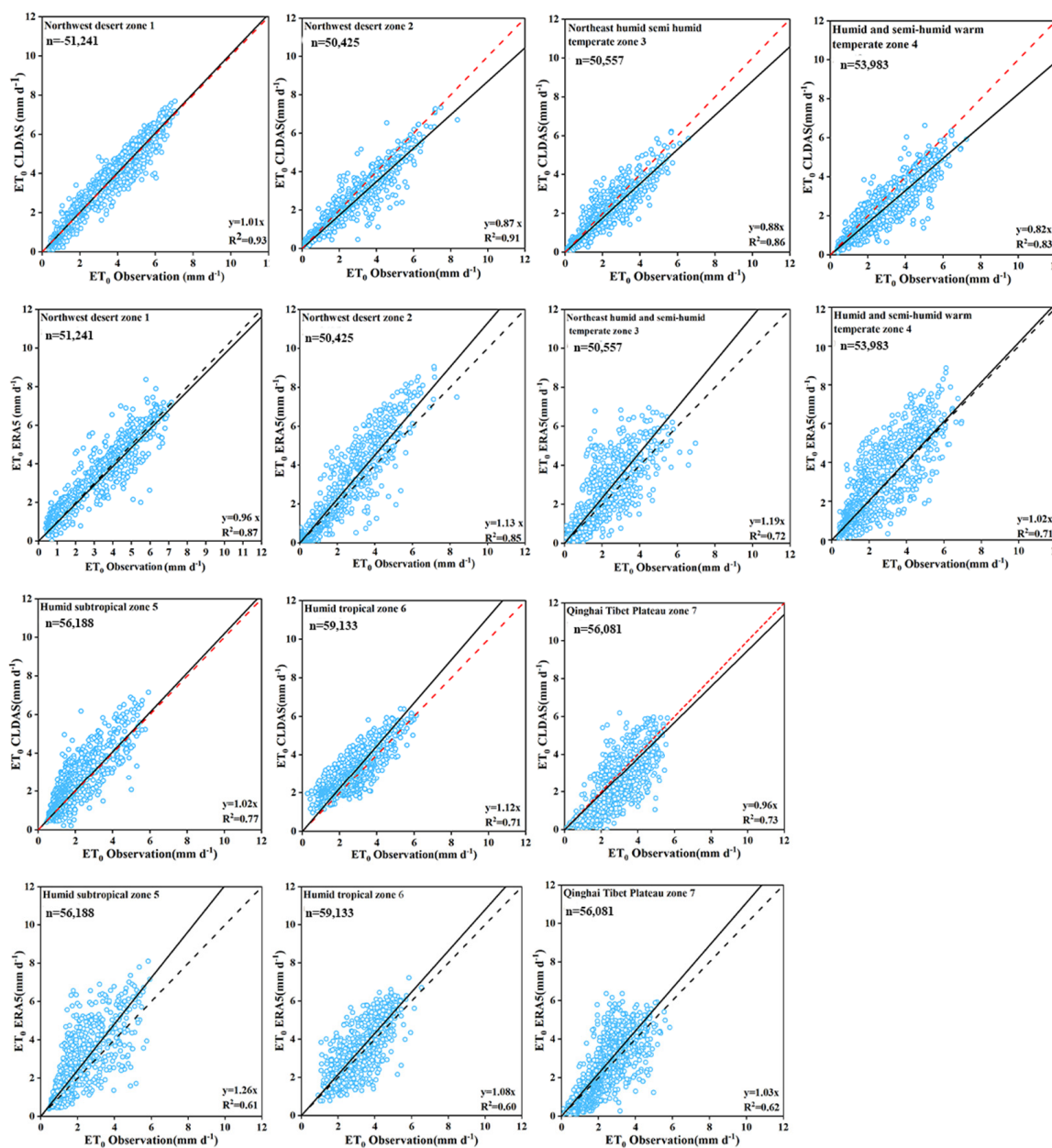

Figure 3. Spatial distribution of the annual mean PM-ET_0 calculated from station observations and CLDAS, ERA5 reanalysis products in China.
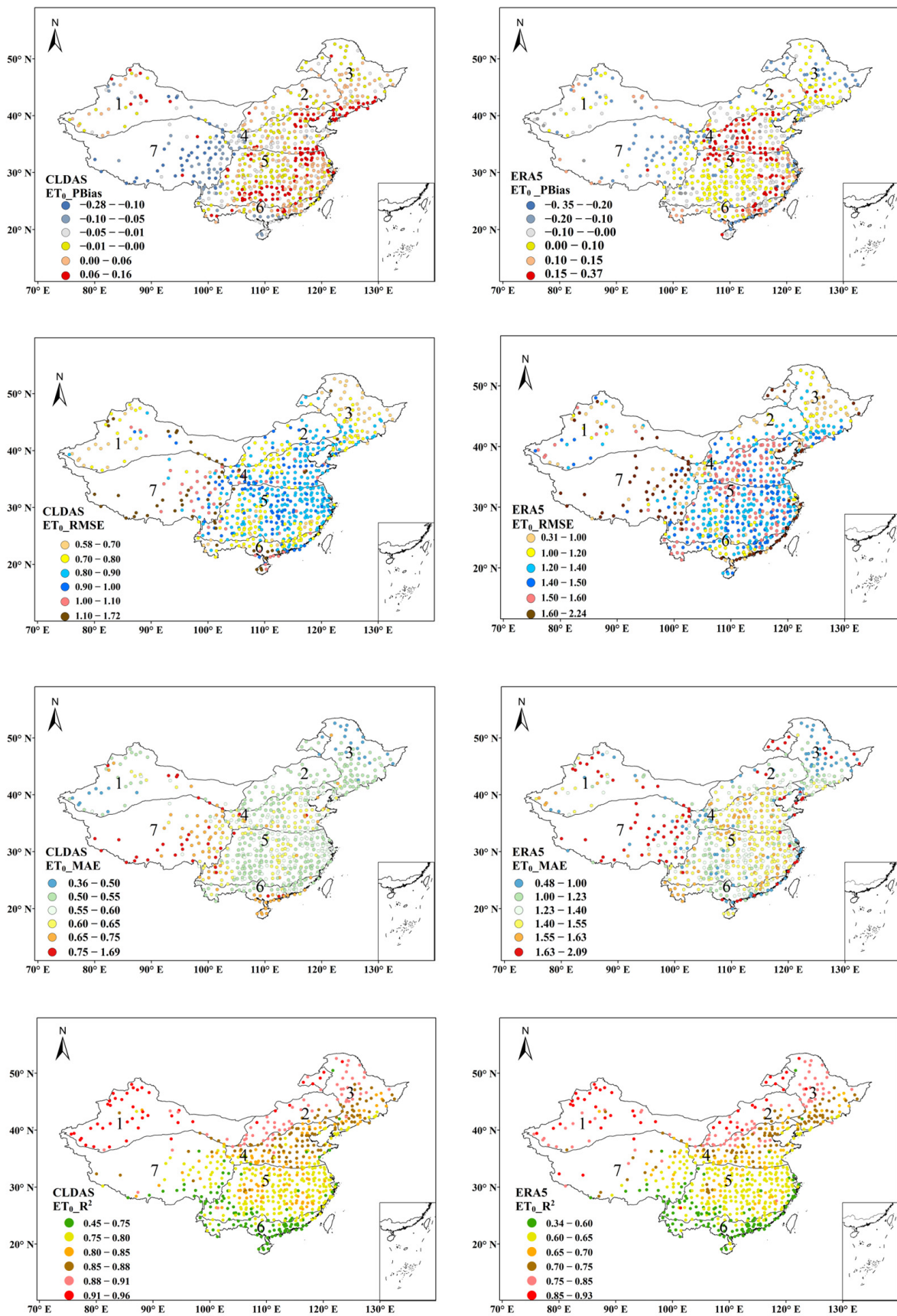
Figure 4. Spatial distribution of PBias, RMSE and R^2 comparing observations and reanalysis estimated PM-ET_0 in various climates with different environments.

Figure 5. Comparing $ET_{0\,Obs}$ with $ET_{0\,CLDAS}$ and $ET_{0\,ERA5}$ on a daily scale, and using CLDAS, ERA5 reanalysis products of seven different climate zones (The blue circle in the figure represents the observed and estimated values, the dashed line is a 1:1 line, and the solid line is a scatter plot fitting curve).

3.3. Assessing the Accuracy of $ET_{0\,CLDAS}$ and $ET_{0\,ERA5}$ Estimates Using Reanalysis Products

The statistical accuracy indicators for the reanalysis estimation of ET_0 and observed ET_0 in the seven climate zones are summarized in Table 6. The results show that the performance of CLDAS in estimating ET_0 is better than that of ERA5 reanalysis products: the average RMSE = 0.91 mm d^{-1} is smaller than that for ERA5 (RMSE = 1.42 mm d^{-1}), while the average determination coefficient is larger for the CLDAS reanalysis products (R^2 = 0.82) than for ERA5 (R^2 = 0.70). Similar results have been shown by Liu et al. (2019) [35], who reported that the simulation results of CLDAS in most climate zones maintained a consistent and reasonable performance. The PBias distribution of ET_0 estimated for two reanalysis products shows that the number of positive bias stations is more than the number of negative bias stations. The $ET_{0\,CLDAS}$ shows a negative bias in climate zones 1,6 and climate

zone 7, with a PBias of -0.05, -0.03 and -0.14, respectively; $ET_{0\,Obs}$ is underestimated in these climate zones. $ET_{0\,CLDAS}$ shows a positive bias in all other climate zones, with a PBias distribution range of 0.01–0.03; $ET_{0\,Obs}$ is overestimated, but to a lesser extent. $ET_{0\,ERA5}$ shows negative bias in climate zones 1,2 and climate zone 7, with PBias ranging from -0.08 to -0.18, and the $ET_{0\,Obs}$ observations are underestimated, the remaining climate zones have a positive PBias and the $ET_{0\,Obs}$ observations are overestimated.

Table 6. Comparing the statistical indicators relative to the estimation of ET_0 by CLDAS. ERA5 reanalysis for 689 weather stations across the seven climatic regions and mainland China.

| Climate Zones	$ET_{0\,CLDAS}$				$ET_{0\,ERA5}$			
	PBias	RMSE	MAE	R^2	PBias	RMSE	MAE	R^2
		mm d^{-1}				mm d^{-1}		
1	-0.05	0.86	0.62	0.91	-0.08	1.33	1.16	0.87
2	0.02	0.82	0.56	0.90	0.07	1.29	1.12	0.85
3	0.01	0.78	0.52	0.88	-0.12	1.12	1.04	0.79
4	0.03	0.89	0.67	0.85	0.16	1.56	1.39	0.70
5	0.01	0.88	0.65	0.77	0.11	1.49	1.30	0.62
6	-0.03	0.91	0.68	0.69	0.13	1.42	1.28	0.54
7	-0.14	1.22	1.06	0.75	-0.18	1.67	1.52	0.59
Average	-0.01	0.91	0.68	0.82	0.01	1.42	1.28	0.70

The results of the ET_0 estimation generated from the two reanalysis datasets revealed that the reanalysis product presented a superior performance in the arid and semi-arid regions, with a higher correlation at most sites, with $R^2 > 0.85$. Like the Northwest desert zone, the Inner Mongolia grassland zone and R^2 of $ET_{0\,CLDAS}$ are 0.91, 0.90, and the R^2 of $ET_{0\,ERA5}$ are 0.87, 0.85, respectively, while the correlations were slightly worse in humid and semi-humid areas such as climate zones 5 and 6. The R^2 distributions of $ET_{0\,CLDAS}$ range from 0.69 to 0.77 and 0.54 to 0.62 for $ET_{0\,ERA5}$ (Table 6).To further evaluate the accuracy of the CLDAS, the ERA5 reanalysis datasets in estimating ET_0, RMSE and MAE for different climate zones are compared. $ET_{0\,CLDAS}$ and $ET_{0\,ERA5}$ have the largest estimation errors in climate zone 7, with an RMSE and MAE of 1.22, 1.06 and 1.67, 1.52, respectively. Except for climate zone 7, the RMSE and MAE of $ET_{0\,CLDAS}$ range from 0.78 to 0.91 and 0.52 to 0.68, respectively, the distribution of the RMSE for $ET_{0\,ERA5}$ ranged from 1.12 to 1.56 and MAE from 1.04 to 1.39. Moreover, the higher values of the RMSE and MAE for ET_0 are mainly concentrated in coastal humid areas such as climate zones 4, 5 and 6 (Figure 6), with an RMSE > 0.88 and MAE > 0.65 for $ET_{0\,CLDAS}$, and $ET_{0\,ERA5}$ with an RMSE > 1.42 and MAE > 1.28. Overall, the RMSE and MAE are shorter and closer to the optimal target when estimating ET_0 using the CLDAS reanalysis products. The effects of topography, slope, monsoon and other factors on meteorological variables in different climatic zones are adopted and integrated into the CLDAS reanalysis datasets, which makes the estimation of $ET_{0\,CLDAS}$ more accurate [35,52].

3.4. Comparison of Time Series Changes in the Monthly Mean Values of the Observed ET_0 and Reanalysis of Estimated ET_0

The monthly time series variation of ET_0 for the seven climate zones across the country in 2017–2019 is shown in Figure 7. The two reanalysis estimates of ET_0 agree well with the observed ET_0 values in most cases, indicating that the reanalysis products capture the seasonal cycle and temporal evolution based on the observed ET_0 to some extent. However, $ET_{0\,ERA5}$ overestimates the fluctuation amplitudes and the estimated ET_0 values are all much higher than the observed values in climate zones 4 and 6. $ET_{0\,ERA5}$ underestimates the fluctuation amplitudes and the estimated ET_0 values are all much lower than the observed values in climate zone 7. In contrast, the $ET_{0\,CLDAS}$ estimates are closer to the observed values in most climate zones.
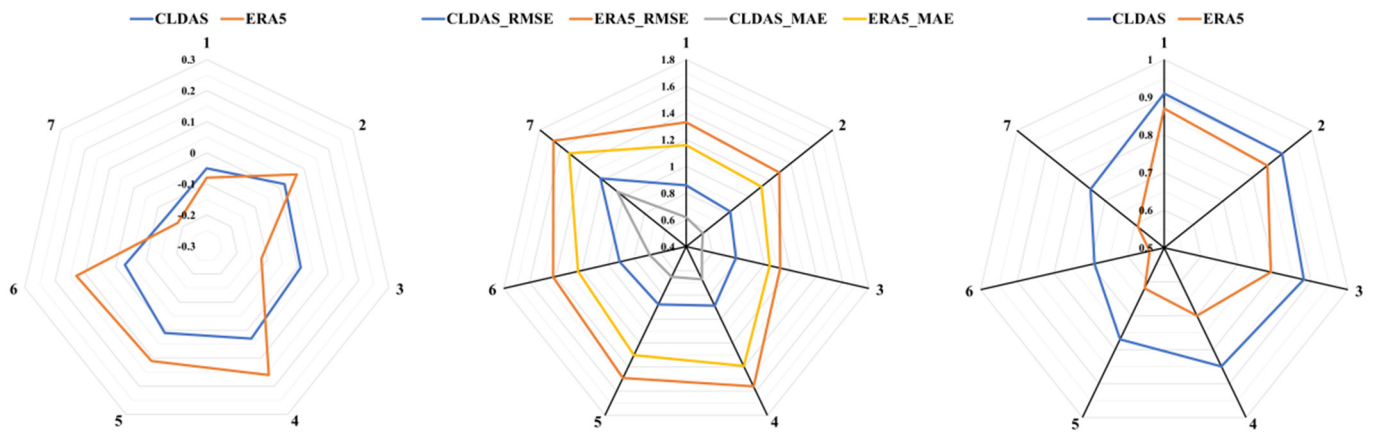
Figure 6. Radar chart of statistical indicators of the PM-ET$_0$ estimated by CLDAS and ERA5 reanalysis across seven climatic regions of China.
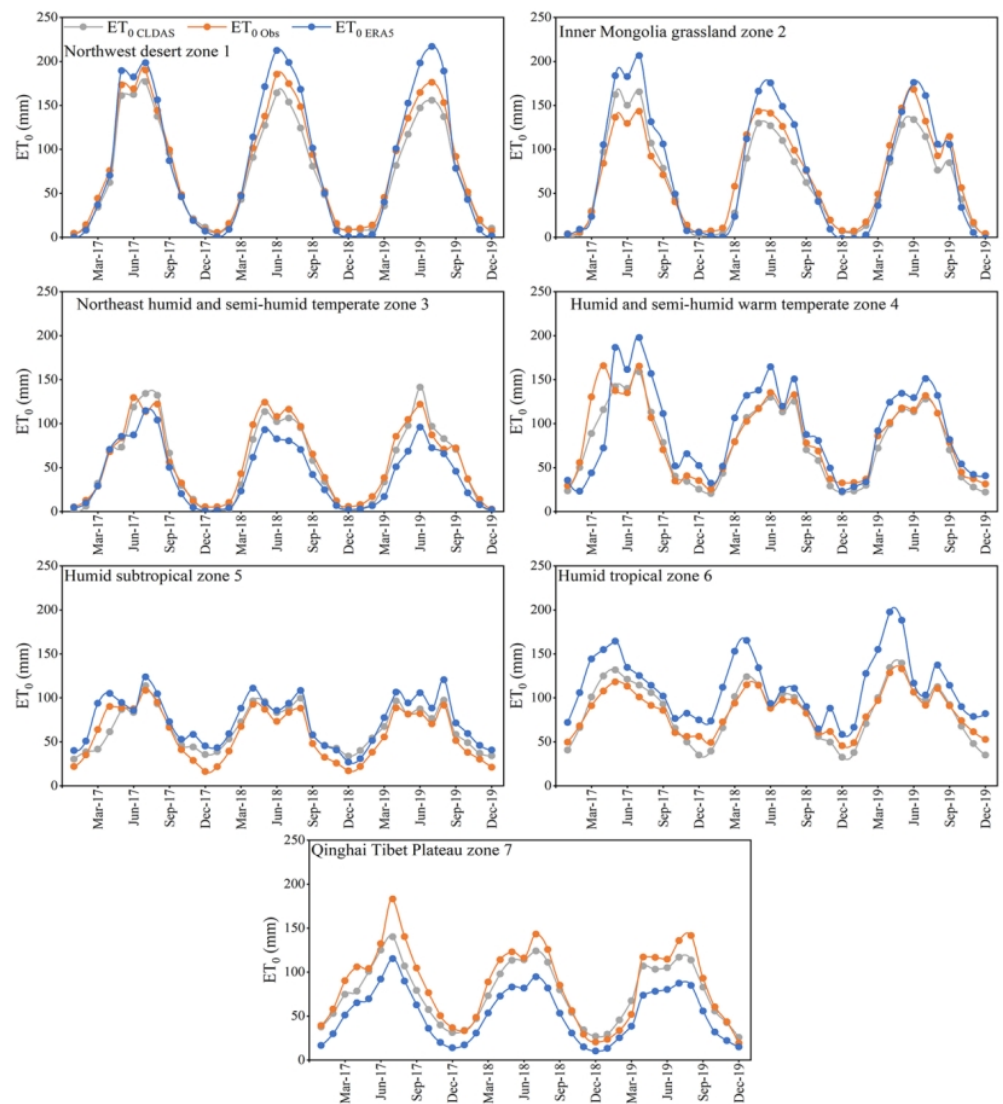
Figure 7. Time series of the monthly PM-ET$_0$ from station observations, CLDAS and ERA5 reanalysis products during the period of 2017–2019 within the seven climates of China.

The calculation of ET$_0$ is affected by meteorological variables such as air temperature, relative humidity and solar radiation, and these meteorological factors vary with time and

region. ET_0 also has obvious seasonal variation and spatial distribution characteristics. The monthly mean ET_0 is large in summer and autumn in different climatic zones, and statistics found that the cumulative ET_0 from May to October each year accounts for about 75–80% of the whole year. ET_0 grows with increased precipitation and temperature during the summer season. Due to the influence of geographical location and meteorological factors, the peak of monthly mean ET_0 occurs at different times, with climate zones 1 and 2 showing a single peak pattern of monthly mean ET_0, with the peak occurring in July each year and the trough occurring in November, lasting until April the following year. There are differences between the annual intervals of monthly mean ET_0 in climate zones 3 and 6, where 2017 showed a single peak type, with a peak in June, and 2018–2019 a double peak type, with a peak in May and a low peak in July. The monthly mean ET_0 in climate zones 4, 5 and 7 show a double peak pattern, with peaks in April and July, and a valley from October to February of the next year.

4. Discussion

4.1. Analysis of Meteorological Variables Related to ET_0 Estimation

In this paper, the key meteorological factors for calculating ET_0 are evaluated. It was found that T_{min} shows an overestimation trend and T_{max} shows an underestimation trend, and the consistency of the reanalysis minimum temperature of the two datasets (average R^2 0.96 and 0.87) is higher than that of the maximum temperature (0.90 and 0.84), but the PBias of the former is larger. Similar conclusions were found by Wu et al. (2022) [53] and Qian et al. (2022) [54] when they used reanalysis data to assess air temperature in the Chinese region. In addition, Simmons et al. (2010) [55] and Paredes et al. [56] also reported a tendency for the overestimation of T_{min} and underestimation of T_{max} by the ERA-Interim in Continental Portugal [57]. The authors hypothesized that CLDAS, ERA5 reanalysis datasets are capturing warming over the land more than over the sea, which makes $T_{min\ CLDAS}$ and $T_{min\ ERA5}$ larger than $T_{min\ Obs}$ data; $T_{max\ CLDAS}$, $T_{max\ ERA5}$ showed the opposite performance. For the reanalysis Rs, both CLDAS and ERA5 slightly overestimate the site-observed Rs, the PBias of $R_{s\ CLDAS}$ and $R_{s\ ERA5}$ range from 0.02 to 0.17 and 0.06 to 0.24, which is similar to the reports of Bojanowski et al. (2014) [57] and Urraca et al. (2017) [58]. Sheffield et al. (2006) [25] also reported a similar conclusion and combined this behavior of overestimation of global radiation for NCEP1 with the fact that the reanalysis dataset does not consider the blocking of shortwave radiation by the clouds. As for reanalysis of the relative humidity, the PBias of RH_{CLDAS} is negative (ranging from −0.07 to −0.30) in the 1–6 climate zones, with a slight underestimation. The PBias of climate zone 7 is positive, and the value is 0.35. This is consistent with the conclusion of Simmons et al. (2010) [55] that the relative humidity of ERA5 reanalysis is underestimated in the mid–low latitudes. Fu et al. (2015) [59] also concluded that the RH of NCEP1 reanalysis was slightly underestimated in Australia. Differently, Martins et al. (2016) [29] reported no tendency for over- or underestimation of the RH when using the reanalysis monthly products for Iberia, which can be attributed to the different time scales of the study. Different from the previous four meteorological factors, the analysis of the wind speed showed a lower accuracy across the seven climatic regions. The average R^2 of $U_{2\ CLDAS}$ was 0.25, and the average R^2 of $U_{2\ ERA5}$ 0.18. Many scholars have reanalyzed the wind speed and obtained similar results, the low accuracy of the wind speed derived from reanalysis was reported by Carvalho et al. (2014) [60] studies applied to Continental Portugal. The same results were reported by Martins et al. (2016) [29] in the Iberian Peninsula for the problem of low accuracy in analyzing the wind speed. The two wind speed estimation alternatives proposed by Allen et al. (1998) [7] are to replace the daily wind speed with the annual average wind speed over the local area or use the world average wind speed value $U_2 = 2$ m s^{-1} as the default wind speed, obtained from over 2000 weather stations worldwide. Jabloun and Sahli (2008) [61] compared the above methods and found that both methods obtained wind speeds with high applicability, but the ET_0 was better estimated using the local area's annual average wind speed.

4.2. Analysis of the Spatial Distribution of the Observation-Calculated ET_0 and Reanalysis-Estimated ET_0

The spatial and frequency distribution of the annual mean values of ET_0 calculated from the station observations, ET_0 estimated by CLDAS and ET_0 estimated by ERA5 in China were analyzed. It was found that the frequency distribution and spatial distribution of different intervals of annual mean evapotranspiration estimated by CLDAS and ERA5 are similar to the observed ET_0, but in most cases, the reanalysis ET_0 is slightly overestimated. The overestimation of the reference evapotranspiration derived from reanalysis has been discovered in many relevant studies. Betts et al. (2009) [62] compared ET_0 at the watershed scale using ERA-Interim reanalysis data and observations, and found that the reference crop evapotranspiration from reanalysis data was significantly larger than the observed value. Moreover, other studies using ERA-Interim reanalysis products also reported an overall overestimation bias for ET_0 [28]. Dee and Uppala (2009, 2011) [44,63] considered that the overestimation of reanalysis data is mainly related to the utilization of small timescale (daily or smaller timescale) reanalysis products, water vapor movement processes and variational bias correction.

4.3. Analysis of the Accuracy of ET_0 Estimated by CLDAS and ERA5 across Different Climatic Regions

Comparing the accuracy of ET_0 estimation across different climatic regions, it was found that the variability of ET_0 in humid and semi-humid areas is higher than that in arid and semi-arid areas. The RMSE of $ET_{0\text{ CLDAS}}$ ranged from 0.78 to 0.82 in climate zones 1–3, the RMSE ranged from 0.89 to 0.91 in climate zones 4–6, the RMSE of $ET_{0\text{ERA5}}$ ranged from 1.12 to 1.33 in climate zones 1–3 and the RMSE ranged from 1.42 to 1.59 in climate zones 4–6. Su et al. (2015) [64] also found that the reanalysis estimates of ET_0 in arid and extremely cold regions are more consistent with the site observations of ET_0. The same trend was found by Zhang et al. (2018) [65] when they used ERA-Interim reanalysis data to study the characteristics of ET_0 in global arid and semi-arid regions. Furthermore, Paredes et al. (2018) [57], using the ERA-Interim reanalysis product for the daily estimation of grass reference evapotranspiration, also found that the higher values of RMSE were mostly concentrated in coastal areas of Portugal. These findings are consistent with the conclusions of this paper. This can be attributed to the meteorological factors related to the estimation of ET_0 in result Section 2.1. We also reported that the accuracy of reanalysis R_s in arid and semi-arid regions is higher than that in humid regions, which is partly because the calculation of solar radiation is a complex task in itself, and the high uncertainty of atmospheric turbidity in humid climatic conditions, which further exacerbates errors between the reanalysis of solar radiation data and station observations, R_s is the most significant meteorological factor affecting ET_0 [66]. The high error of the reanalysis R_s leads to a high variability of ET_0 in humid and semi-humid climate zones.

5. Summary and Conclusions

It is difficult to obtain long timeseries meteorological variables required for PM-ET_0 calculation from ground stations. The reanalysis datasets provide all the weather variables required for calculating ET_0, but needs to be evaluated for accuracy. In this paper, meteorological factors such as T_{min} and T_{max}, R_s, RH and U_2 derived from CLDAS and ERA5 are statistically analyzed. Moreover, based on the daily meteorological data of 689 surface meteorological stations covering seven different climatic regions in China, $ET_{0\text{ CLDAS}}$ and $ET_{0\text{ ERA5}}$ at different timescales are compared and evaluated.

The quality of meteorological factors for calculating PM-ET_0 obtained from CLDAS and ERA5 reanalysis products is acceptable, and the correlation between reanalysis temperature and station observation temperature is high, with $R^2 > 0.90$ for $T_{min\text{ CLDAS}}$, $T_{max\text{ CLDAS}}$, and $R^2 > 0.84$ for $T_{min\text{ ERA5}}$, $T_{max\text{ ERA5}}$; however, there is a tendency for an underestimation of T_{max}, and conversely, a tendency for an overestimation of T_{min}. R_s and RH can be accurately estimated from reanalysis datasets, but reanalysis R_s has a slight overestimation trend for site observation R_s and an underestimation trend for site observation RH. Com-

pared with the ERA5 reanalysis products, T_{min}, T_{max}, R_s and RH derived from the CLDAS products are closer to the site observations, and the overall RMSE and MAE values are smaller. In contrast, the accuracy of both $U_{2\,CLDAS}$ and $U_{2\,ERA5}$ is coarser, but the reanalysis of wind speed does not cause a large variability in ET_0.

Two reanalysis products capture the seasonal cycle and monthly time evolution based on the observed ET_0. During the year, 75–80% of ET_0 is concentrated in April–October, but the monthly mean ET_0 in different climate zones shows single-peak and double-peak type variations, with different peak occurrence times. In addition, the agreement between the reanalysis estimated ET_0 and site-observed ET_0 is high in arid and semi-arid areas, with the lowest value of $ET_{0\,CLDAS}$ correlation coefficient being 0.90 and $ET_{0\,ERA5}$ 0.85. The consistency is slightly worse in wet and semi-humid areas, with the R^2 variation range of 0.69–0.88 for $ET_{0\,CLDAS}$ and 0.54–0.79 for $ET_{0\,ERA5}$. CLDAS reanalyzed meteorological variables which are used to compute the PM-ET_0, and estimated ET_0 closer to the site observation $ET_{0\,Obs}$, comparing the corresponding values of ERA5.

These results suggest that reanalysis weather products (R_s, T_{max}, T_{min}, RH and U_2) can be used to estimate ET_0 when the observed weather data are unavailable. However, the causes of the impact of errors in each weather variable on the accuracy of the estimated ET_0 are not clear, and further studies are required to clarify the quantitative sensitivity of the errors in the reanalysis weather variables on the estimated ET_0 as a way to decrease the reanalysis product estimation errors obtained when using daily time steps. Moreover, studies are needed to combine long past series data with forecasts, to achieve the real-time operation of irrigation scheduling models.

Author Contributions: Conceptualization, X.Y. and L.Q.; methodology, X.Y., W.W. and L.Q.; data curation, X.Y. and X.H. (Xuefei Huo); writing—original draft preparation, X.Y., L.Q., X.H. (Xiaotao Hu) and Y.W.; writing—review and editing, X.Y., L.Q., W.W. and X.H. (Xuefei Huo); project administration, X.Y. and L.Q. All authors have read and agreed to the published version of the manuscript.

Data Availability Statement: Not applicable.

Conflicts of Interest: The authors declare no conflict of interest. The funders had no role in the design of the study; in the collection, analysis, or interpretation of data; in the writing of the manuscript, or in the decision to publish the results.

References

1. Holdridge, L.R. *Life Zone Ecology*; Tropical Science: San Jose, Costa Rica, 1967.
2. Pereira, L.S.; Perrier, A.; Allen, R.G.; Alves, I. Evapotranspiration: Review of concepts and future trends. *J. Irrig. Drain Eng.* **1999**, *125*, 45–51. [CrossRef]
3. Pereira, L.S.; Allen, R.G.; Smith, M.; Raes, D. Crop evapotranspiration estimation with FAO56: Past and future. *Agric. Water Manag.* **2015**, *147*, 4–20. [CrossRef]
4. Scanlon, B.R.; Faunt, C.C.; Longuevergne, L.; Reedy, R.C.; Alley, W.M.; McGuire, V.L.; McMahon, P.B. Groundwater depletion and sustainability of irrigation in the US High Plains and Central Valley. *Proc. Natl. Acad. Sci. USA* **2012**, *109*, 9320–9325. [CrossRef] [PubMed]
5. Feng, Y.; Peng, Y.; Cui, N.; Gong, D.; Zhang, K. Modeling reference evapotranspiration using extreme learning machine and generalized regression neural network only with temperature data. *Comput. Electron. Agric.* **2017**, *136*, 71–78. [CrossRef]
6. Dong, Y.; Zhao, Y.; Zhai, J.; Zhao, J.S.; Han, J.Y.; Wang, Q.M.; He, G.H. Changes in reference evapotranspiration over the non-monsoon region of China during 1961–2017: Relationships with atmospheric circulation and attributions. *Int. J. Clim.* **2020**, *41*, E734–E751. [CrossRef]
7. Allen, R.G.; Pereira, L.S.; Raes, D.; Smith, M. *Crop Evapotranspiration: Guidelines for Computing Crop Water Requirements*; Food and Agriculture Organization of the United Nations: Rome, Italy, 1998.

8. Valiantzas, J.D. Simplified forms for the standardized FAO-56 Penman–Monteith reference evapotranspiration using limited weather data. *J. Hydrol.* **2013**, *505*, 13–23. [CrossRef]

9. Pereira, L.S.; Paredes, P.; Rodrigues, G.C.; Neves, M. Modeling malt barley water use and evapotranspiration partitioning in two contrasting rainfall years. Assessing AquaCrop and SIMDualKc models. *Agric. Water Manag.* **2015**, *159*, 239–254. [CrossRef]

10. Jensen, M.E.; Allen, R.G. *Evaporation, Evapotranspiration, and Irrigation Water Requirements*; American Society of Civil Engineers: Reston, VA, USA, 2016. [CrossRef]

11. Monteith, J.L. Evaporation and the Environment in the State and Movement of Water in Living Organisms. *Symp. Soc. Exp. Biol.* **1965**, *19*, 205–234.

12. Popova, Z.; Kercheva, M.; Pereira, L.S. Validation of the FAO methodology for computing ETo with limited data. Application to south Bulgaria. *Irrig. Drain.* **2006**, *55*, 201–215. [CrossRef]

13. McMahon, T.A.; Finlayson, B.L.; Peel, M.C. Historical developments of models for estimating evaporation using standard meteorological data. *Wiley Interdiscip. Rev. Water* **2016**, *3*, 788–818. [CrossRef]

14. Martínez-Cob, A.; Tejero-Juste, M. A wind-based qualitative calibration of the Hargreaves ET0 estimation equation in semiarid regions. *Agric. Water Manag.* **2004**, *64*, 251–264. [CrossRef]

15. Eyer, J.R. *Progress Achieved on Assimilation of Satellite Data in Numerical Weather Prediction over the Last 30 Years/Proceeding of ECMWF Seminar on Recent Developments in of Satellite Observations in Numerical Weather Prediction*; ECMWF Publication: Reading, UK, 2007; pp. 1–27.

16. Eyre, J.R.; Kelly, G.A.; McNally, A.P.; Andersson, E.; Persson, A. Assimilation of TOVS radiance information through one-dimensional variational analysis. *Q. J. R. Meteorol. Soc.* **1993**, *119*, 1427–1463. [CrossRef]

17. Harris, B.A.; Kelly, G. A satellite radiance-bias correction scheme for data assimilation. *Q. J. R. Meteorol. Soc.* **2001**, *127*, 1453–1468. [CrossRef]

18. Wang, Y.; Han, W.; Xue, J.; Li, J.; Lei, B.; Yang, J. Adaptive tuning of background error and satellite radiance observation error for operational variational assimilation. In *MIPPR 2007: Remote Sensing and GIS Data Processing and Applications; and Innovative Multispectral Technology and Applications*; SPIE: Washington, DC, USA, 2007; Volume 6790, pp. 1063–1071. [CrossRef]

19. Fick, S.E.; Hijmans, R.J. WorldClim 2: New 1-km spatial resolution climate surfaces for global land areas. *Int. J. Climatol.* **2017**, *37*, 4302–4315. [CrossRef]

20. Trouet, V.; Van Oldenborgh, G.J. KNMI Climate Explorer: A Web-Based Research Tool for High-Resolution Paleoclimatology. *Tree-Ring Res.* **2013**, *69*, 3–13. [CrossRef]

21. Balsamo, G.; Albergel, C.; Beljaars, A.; Boussetta, S.; Brun, E.; Cloke, H.; Dee, D.; Dutra, E.; Muñoz-Sabater, J.; Pappenberger, F.; et al. ERA-Interim/Land: A global land surface reanalysis data set. *Hydrol. Earth Syst. Sci.* **2015**, *19*, 389–407. [CrossRef]

22. Kanamitsu, M.; Ebisuzaki, W.; Woollen, J.; Yang, S.-K.; Potter, G.L. NCEP–DOE AMIP-II Reanalysis (R-2). *Bull. Am. Meteorol. Soc.* **2002**, *83*, 1631–1644. [CrossRef]

23. Kazutoshi, O.; Junichi, T.; Hiroshi, K.; Masami, S.; Shinya, K.; Hiroaki, H.; Takanori, M.; Nobuo, Y.; Hirotaka, K. The JRA-25 Reanalysis. *J. Meteorol. Soc. Jpn.* **2007**, *85*, 369–432. [CrossRef]

24. Kobayashi, S.; Ota, Y.; Harada, Y.; Ebita, A.; Moriya, M.; Onoda, H.; Onogi, K.; Kamahori, H.; Kobayashi, C.; Endo, H.; et al. The JRA-55 Reanalysis: General Specifications and Basic Characteristics. *J. Meteorol. Soc. Jpn. Ser. II* **2015**, *93*, 5–48. [CrossRef]

25. Sheffield, J.; Goteti, G.; Wood, E.F. Development of a 50-Year High-Resolution Global Dataset of Meteorological Forcings for Land Surface Modeling. *J. Clim.* **2006**, *19*, 3088–3111. [CrossRef]

26. Martí, B.; Jose, U.; Giovanni, L.; Philipp, K.; Álvaro, N.; Rolando, C. Validation of ERA5-Land temperature and relative humidity on four Peruvian glaciers using on-glacier observations. *J. Mt. Sci.* **2022**, *19*, 1849–1873. [CrossRef]

27. Song, H.Q.; Sun, X.L.; Li, Y.P. Evaluation of ERA5 reanalysis soil moisture over inner mongolia. *Sci. Technol. Eng.* **2020**, *20*, 2161–2168.

28. Srivastava, P.K.; Han, D.; Islam, T.; Petropoulos, G.P.; Gupta, M.; Dai, Q. Seasonal evaluation of evapotranspiration fluxes from MODIS satellite and mesoscale model downscaled global reanalysis datasets. *Theor. Appl. Clim.* **2016**, *124*, 461–473. [CrossRef]

29. Martins, D.S.; Paredes, P.; Raziei, T.; Pires, C.; Cadima, J.; Pereira, L.S. Assessing reference evapotranspiration estimation from reanalysis weather products. An application to the Iberian Peninsula. *Int. J. Clim.* **2016**, *37*, 2378–2397. [CrossRef]

30. Zhao, T.; Guo, W.; Fu, C. Calibrating and Evaluating Reanalysis Surface Temperature Error by Topographic Correction. *J. Clim.* **2008**, *21*, 1440–1446. [CrossRef]

31. Hwang, S.; Graham, W.D.; Geurink, J.S.; Adams, A. Hydrologic implications of errors in bias-corrected regional reanalysis data for west central Florida. *J. Hydrol.* **2014**, *510*, 513–529. [CrossRef]

32. Liu, Y.; Shi, C.X.; Wang, H.J.; Han, S. Applicability assessment of CLDAS temperature data in China. *Atmos. Sci.* **2021**, *44*, 540–548. [CrossRef]

33. Shi, C.; Xie, Z.; Qian, H.; Liang, M.; Yang, X. China land soil moisture EnKF data assimilation based on satellite remote sensing data. *Sci. China Earth Sci.* **2011**, *54*, 1430–1440. [CrossRef]

34. Yang, F.; Lu, H.; Yang, K.; He, J.; Wang, W.; Wright, J.S.; Li, C.; Han, M.; Li, Y. Evaluation of multiple forcing data sets for precipitation and shortwave radiation over major land areas of China. *Hydrol. Earth Syst. Sci.* **2017**, *21*, 5805–5821. [CrossRef]

35. Liu, J.; Shi, C.; Sun, S.; Liang, J.; Yang, Z.-L. Improving Land Surface Hydrological Simulations in China Using CLDAS Meteorological Forcing Data. *J. Meteorol. Res.* **2019**, *33*, 1194–1206. [CrossRef]

36. Cui, Y.Y.; Qin, J.; Jing, W.; Tan, G. Applicability evaluation of merged soil moisture in GLDAS and CLDAS products over Qinghai-Tibetan Plateau. *Plateau Meteorol.* **2018**, *37*, 123–136. [CrossRef]

37. Shi, C.; Zhang, S.; Sun, S. Effect of Improved Precipitation CLDAS on Snow Simulation in China. *Meteor. Mon.* **2018**, *44*, 985–997. [CrossRef]

38. Vanella, D.; Longo-Minnolo, G.; Belfiore, O.R.; Ramírez-Cuesta, J.M.; Pappalardo, S.E.; Consoli, S.; D'urso, G.; Chirico, G.B.; Coppola, A.; Comegna, A.; et al. Comparing the use of ERA5 reanalysis dataset and ground-based agrometeorological data under different climates and topography in Italy. *J. Hydrol.* **2022**, *42*, 101182. [CrossRef]

39. Shea, J.G.; Worley, J.; Stern, R.N. *An Introduction to Atmospheric and Oceanographic Datasets. (No.NCAR/TN-404+IA)*; University Corporation for Atmospheric Research: Boulder, CO, USA, 1994. [CrossRef]

40. Sheffield, J.; Wood, E.F.; Roderick, M.L. Little change in global drought over the past 60 years. *Nature* **2012**, *491*, 435–438. [CrossRef]

41. Boulard, D.; Castel, T.; Camberlin, P. Capability of a regional climate model to simulate climate variables requested for water balance computation: A case study over northeastern France. *Clim. Dyn.* **2015**, *46*, 2689–2716. [CrossRef]

42. Paredes, P.; Rodrigues, G.C.; Alves, I.; Pereira, L.S. Partitioning evapotranspiration, yield prediction and economic returns of maize under various irrigation management strategies. *Agric. Water Manag.* **2014**, *135*, 27–39. [CrossRef]

43. Shi, C.X.; Jiang, L.P.; Zhang, T.; Xu, B.; Han, S. Status and plans of CMA land data assimilation system (CLDAS) project. *Geophys. Res. Abstr.* **2014**, *16*, EGU2014-5671.

44. Dee, D.P.; Uppala, S.M.; Simmons, A.J. The ERA-Interim reanalysis: Configuration and performance of the data assimilation system. *Q. J. R. Meteorol. Soc.* **2011**, *137*, 553–597. [CrossRef]

45. Allen, R.G.; Smith, M.; Perrier, A.; Pereira, L.S. An update for the definition of reference evapotranspiration. *ICID Bull.* **1994**, *43*, 1–35.

46. Takakura, T.; Kubota, C.; Sase, S.; Hayashi, M.; Ishii, M.; Takayama, K.; Nishina, H.; Kurata, K.; Giacomelli, G.A. Measurement of evapotranspiration rate in a single-span greenhouse using the energy-balance equation. *Biosyst. Eng.* **2009**, *102*, 298–304. [CrossRef]

47. Mobilia, M.; Longobardi, A. Prediction of Potential and Actual Evapotranspiration Fluxes Using Six Meteorological Data-Based Approaches for a Range of Climate and Land Cover Types. *ISPRS Int. J. Geo Inf.* **2021**, *10*, 192. [CrossRef]

48. Yin, Y.H.; Li, B.Y. A New Scheme for Climate Regionalization in China. *Acta Geogr. Sin.* **2010**, *65*, 3–12. [CrossRef]

49. Zheng, J.Y.; Bian, J.J.; Ge, Q.S.; Hao, Z.X.; Yin, Y.H.; Liao, Y.M. The climate regionalization in China for 1981–2010. *Geogr. Res.* **2013**, *32*, 987–997.

50. Nash, J.E.; Sutcliffe, J.V. River flow forecasting through conceptual models part I—A discussion of principles. *J. Hydrol.* **1970**, *10*, 282–290. [CrossRef]

51. Gupta, H.V.; Sorooshian, S.; Yapo, P.O. Status of Automatic Calibration for Hydrologic Models: Comparison with Multilevel Expert Calibration. *J. Hydrol. Eng.* **1999**, *4*, 135–143. [CrossRef]

52. Tie, R.; Shi, C.; Wan, G.; Hu, X.J.; Kang, L.H.; Ge, L.L. CLDASSD: Reconstructing Fine Textures of the Temperature Field Using Super-Resolution Technology. *Adv. Atmos. Sci.* **2022**, *39*, 117–130. [CrossRef]

53. Wu, L.; Qian, L.; Huang, G.; Liu, X.-G.; Wang, Y.-C.; Bai, H.; Wu, S.-F. Assessment of Daily of Reference Evapotranspiration Using CLDAS Product in Different Climate Regions of China. *Water* **2022**, *14*, 1744. [CrossRef]

54. Qian, L.; Wu, L.F.; Liu, X.G.; Cui, Y.K.; Wang, Y.W. Comparison of CLDAS and Machine Learning Models for Reference Evapotranspiration Estimation under Limited Meteorological Data. *Sustainability* **2022**, *14*, 14577. [CrossRef]

55. Simmons, A.J.; Willett, K.M.; Jones, P.D.; Thorne, P.W.; Dee, D.P. Low-frequency variations in surface atmospheric humidity, temperature, and precipitation: Inferences from reanalyses and monthly gridded observational data sets. *J. Geophys. Res.* **2010**, *115*, D01110. [CrossRef]

56. Paredes, P.; Martins, D.S.; Pereira, L.S.; JorgePires, C. Accuracy of daily estimation of grass reference evapotranspiration using ERA-Interim reanalysis products with assessment of alternative bias correction schemes. *Agric. Water Manag.* **2018**, *210*, 340–353. [CrossRef]

57. Bojanowski, J.S.; Vrieling, A.; Skidmore, A.K. A comparison of data sources for creating a long-term time series of daily gridded solar radiation for Europe. *Sol. Energy* **2014**, *99*, 152–171. [CrossRef]

58. Urraca, R.; Martinez-De-Pison, E.; Sanz-Garcia, A.; Antonanzas, J.; Antonanzas-Torres, F. Estimation methods for global solar radiation: Case study evaluation of five different approaches in central Spain. *Renew. Sustain. Energy Rev.* **2017**, *77*, 1098–1113. [CrossRef]

59. Fu, G.; Charles, S.P.; Timbal, B.; BranislavaOuyang, F. Comparison of NCEP-NCAR and ERA-Interim over Australia. *Int. J. Clim.* **2015**, *36*, 2345–2367. [CrossRef]

60. Carvalho, D.; Rocha, A.; Gómez-Gesteira, M.; Santos, C.S. WRF wind simulation and wind energy production estimates forced by different reanalyses: Comparison with observed data for Portugal. *Appl. Energy* **2013**, *117*, 116–126. [CrossRef]

61. Jabloun, M.; Sahli, A. Evaluation of FAO-56 methodology for estimating reference evapotranspiration using limited climatic data. *Agric. Water Manag.* **2008**, *95*, 707–715. [CrossRef]

62. Betts, A.K.; Köhler, M.; Zhang, Y. Comparison of river basin hydrometeorology in ERA-Interim and ERA-40 reanalyses with observations. *J. Geophys. Res.* **2009**, *114*, D02101. [CrossRef]

63. Dee, D.P.; Uppala, S. Variational bias correction of satellite radiance data in the ERA-Interim reanalysis. *Q. J. R. Meteorol. Soc.* **2009**, *135*, 1830–1841. [CrossRef]
64. Su, T.; Feng, T.; Feng, G. Evaporation variability under climate warming in five reanalyses and its association with pan evaporation over China. *J. Geophys. Res. Atmos.* **2015**, *120*, 8080–8098. [CrossRef]
65. Zhang, X.; Li, M.; Ma, Z. Evapotranspiration variability over global arid and semi-arid regions from 1982 to 2011. *Chin. J Atmos. Sci.* **2018**, *42*, 251–267. [CrossRef]
66. Luo, H.; Cui, Y.; Duan, Z. Analysis of the Sensitivity of ET0 and the Main Meteorological Factors in Major Agricultural Regions in Tibet. *Mod. Water Sav. Effic. Agric. Ecol. Irrig. Area Constr China* **2010**, *8*, 130–136.